Supporting Information

Selective photocatalytic conversion of lignin via metal-doped anodic TiO_2 nanotubes

Sabiha Sultana[1*], Krzysztof Szczubiałka[1], Marcin Pisarek[2], Grzegorz D. Sulka[1], Karolina Syrek[1*]

[1]Jagiellonian University, Department of Physical Chemistry and Electrochemistry

Gronostajowa 2, 30 - 387 Krakow, Poland

[2]Laboratory of Surface Analysis, Institute of Physical Chemistry, Polish Academy of Sciences, Kasprzaka 44/52, 01-224 Warsaw, Poland

Keywords: nanotube array, doping, photoelectrochemical oxidation, lignin,

* Corresponding author. E-mail: sabihasultana135@gmail.com (S.S.); syrek@chemia.uj.edu.pl; karolina.syrek@uj.edu.pl (K.S.)

Jagiellonian University, Faculty of Chemistry, Department of Physical Chemistry & Electrochemistry

Gronostajowa 2, 30387 Krakow, Poland

1. Morphology of studied materials

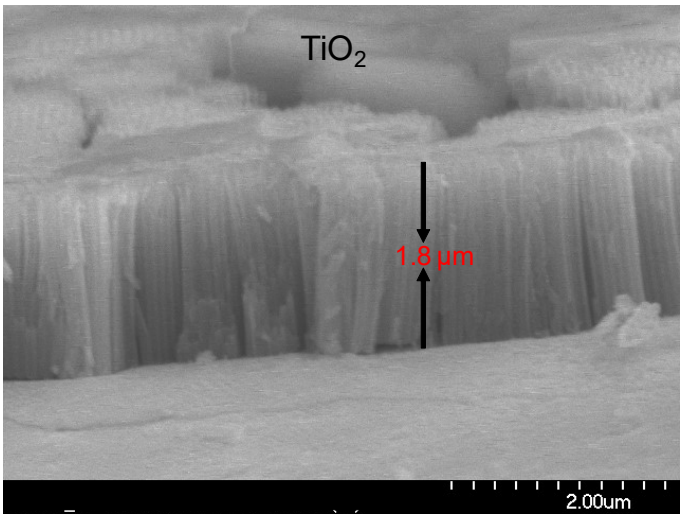

Figure S1. Cross-sectional FESEM image of TiO_2 NTs.

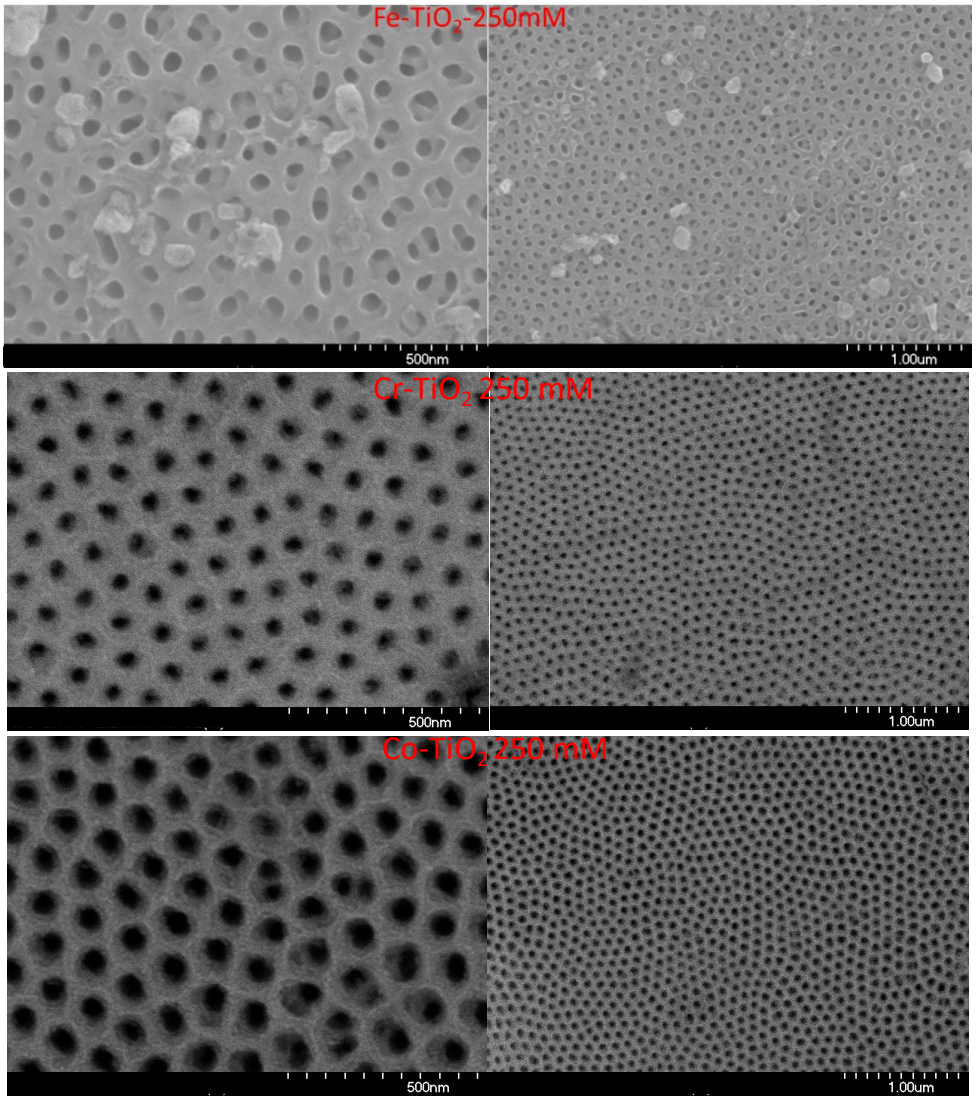

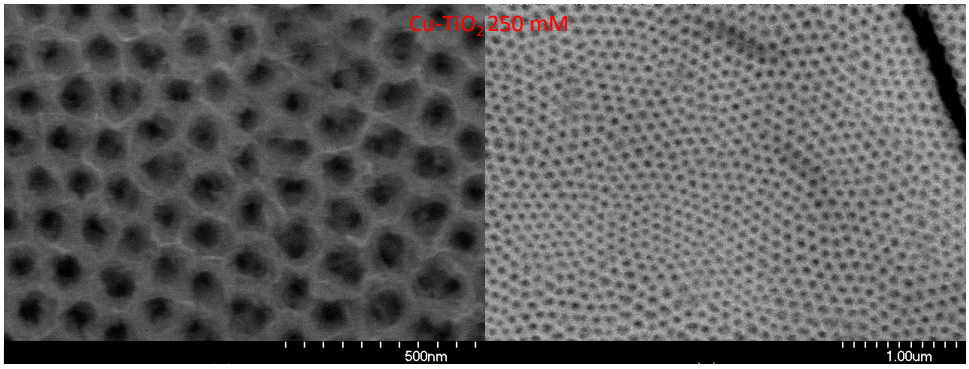

Figure S2. FESEM images of Fe-, Cr-, Co-, and Cu-doped TiO_2 NTs synthesized in the electrolyte with a higher concentration of the metal fluoride salt (250 mM).

Table S1. Average dopant content estimated from EDS spectra.

Material	Metal content (at.%)
Fe-TiO₂	0.23 ± 0.08
Cu-TiO₂	0.69 ± 0.18
Co-TiO₂	0.71 ± 0.13
Cr-TiO₂	0.52 ± 0.15

2. Crystalline structure

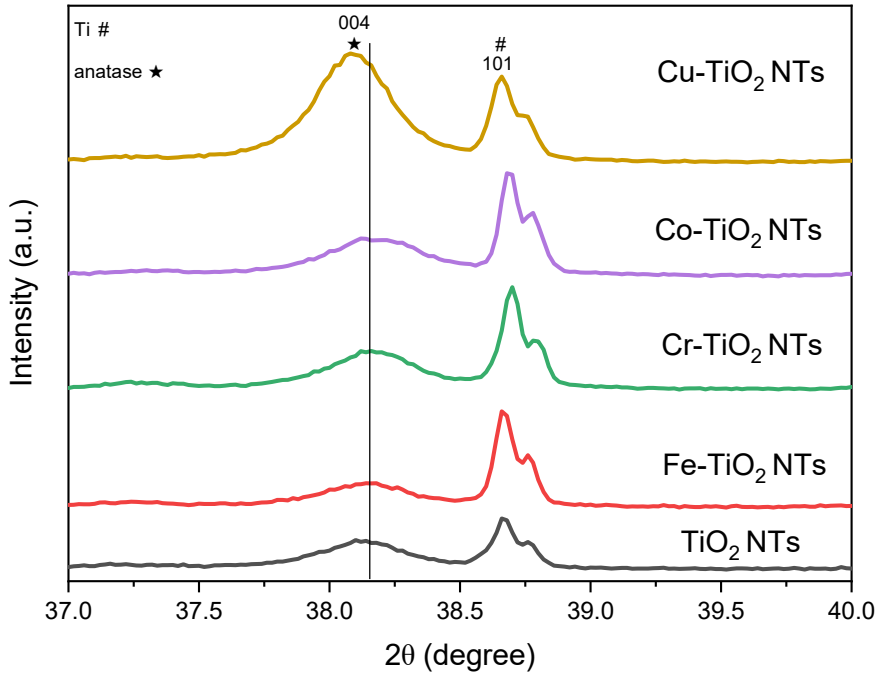

Figure S3. Zoomed-in views of the (004) diffraction peak of pristine and metal-doped TiO_2 NTs.

3. Optical properties

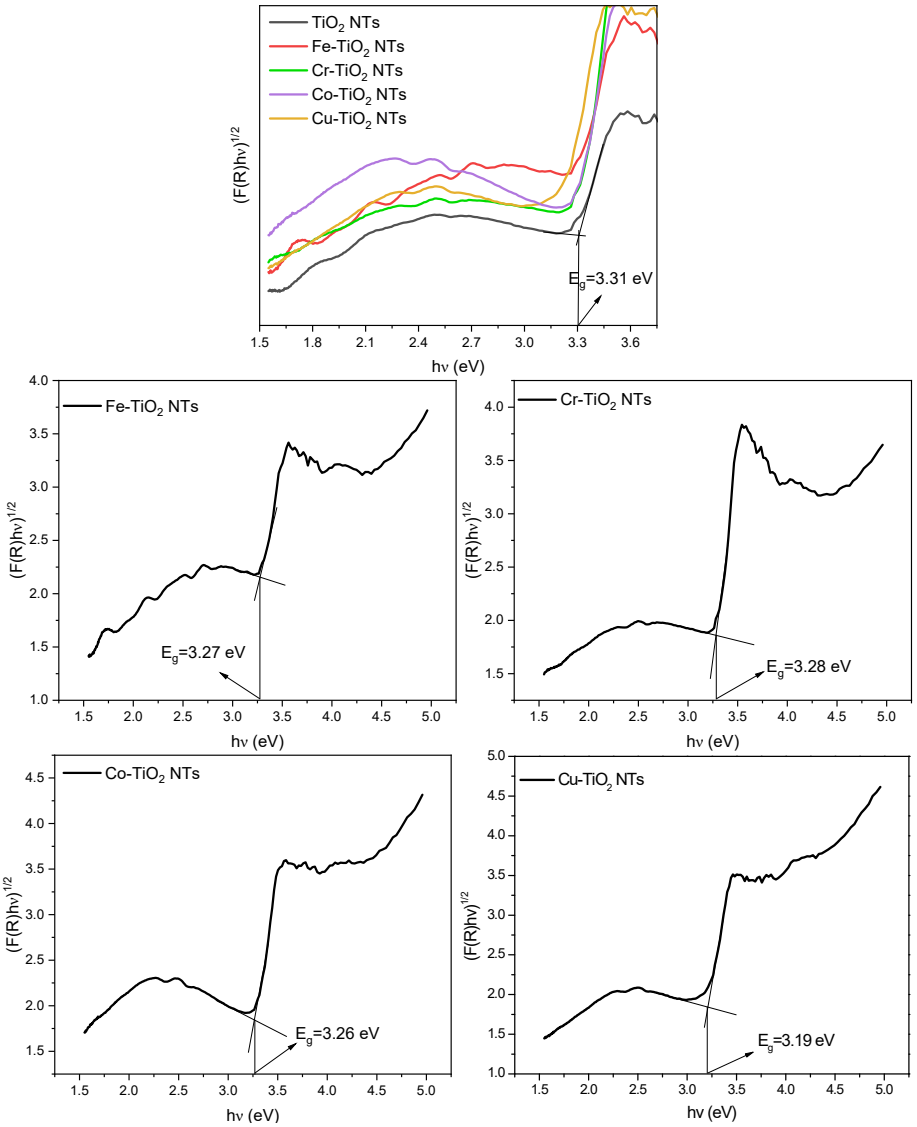

Figure S4. Tauc's plots for pristine and metal-doped TiO_2 NTs.

4. XPS measurements

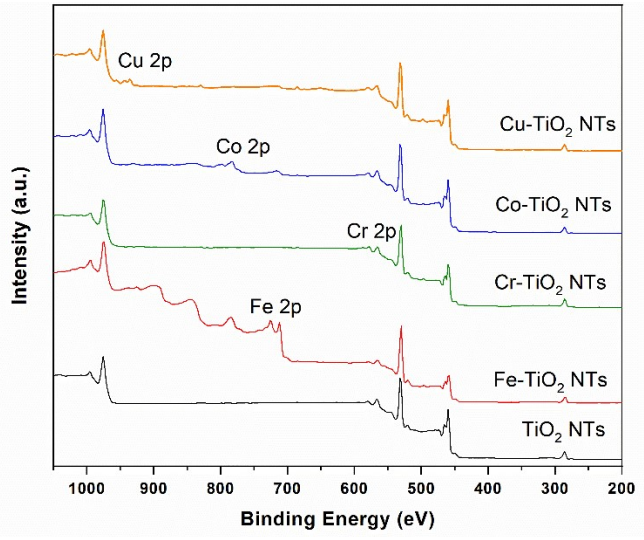

Figure S5. XPS survey spectra for pristine and doped TiO_2 NTs.

5. PEC characterization

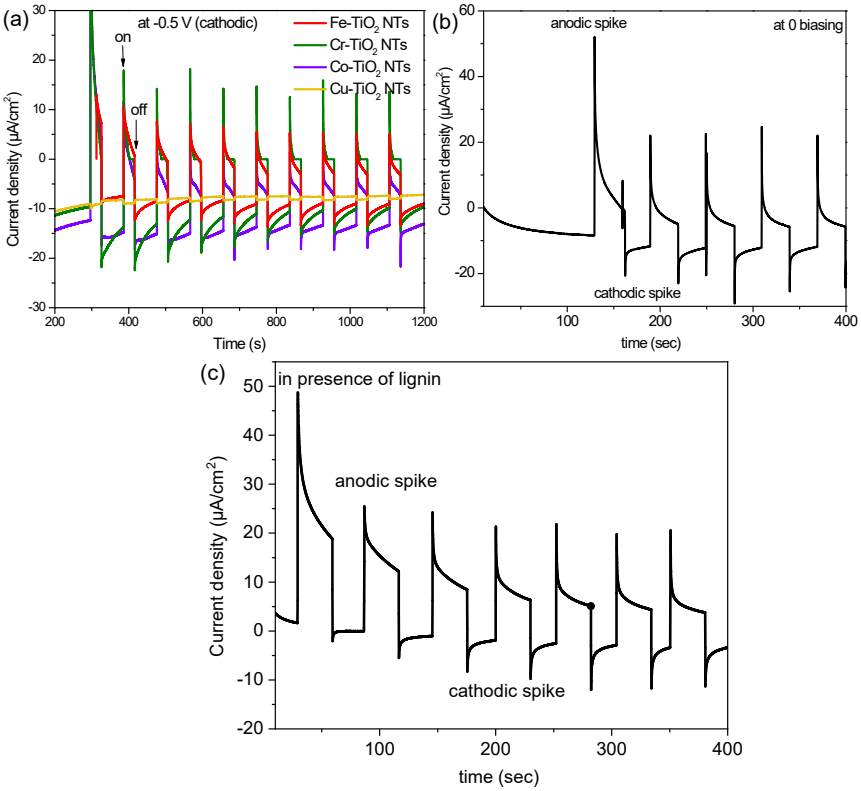

Figure S6. Light on-off I-t curve of different metal-doped TiO_2 NTs at applied negative bias (a), Cu-TiO_2 NTs at zero bias in the absence (b) and in the presence (c) of lignin in KNO_3.

6. EIS studies

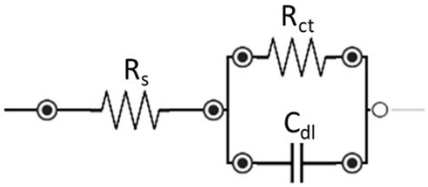

	TiO_2 NT	Fe-TiO_2 NT	Cr-TiO_2 NT	Co-TiO_2 NT	Cu-TiO_2 NT
Rs (Ω)	33.1	30.9	29.9	31.1	35.1
Rct (Ω)	1993	1739	1643	1980	2328
C (nF)	3119	3202	3218	3193	2631

Figure S7. EIS fitted equivalent circuit and corresponding fitting data.

7. HPLC-MS analysis

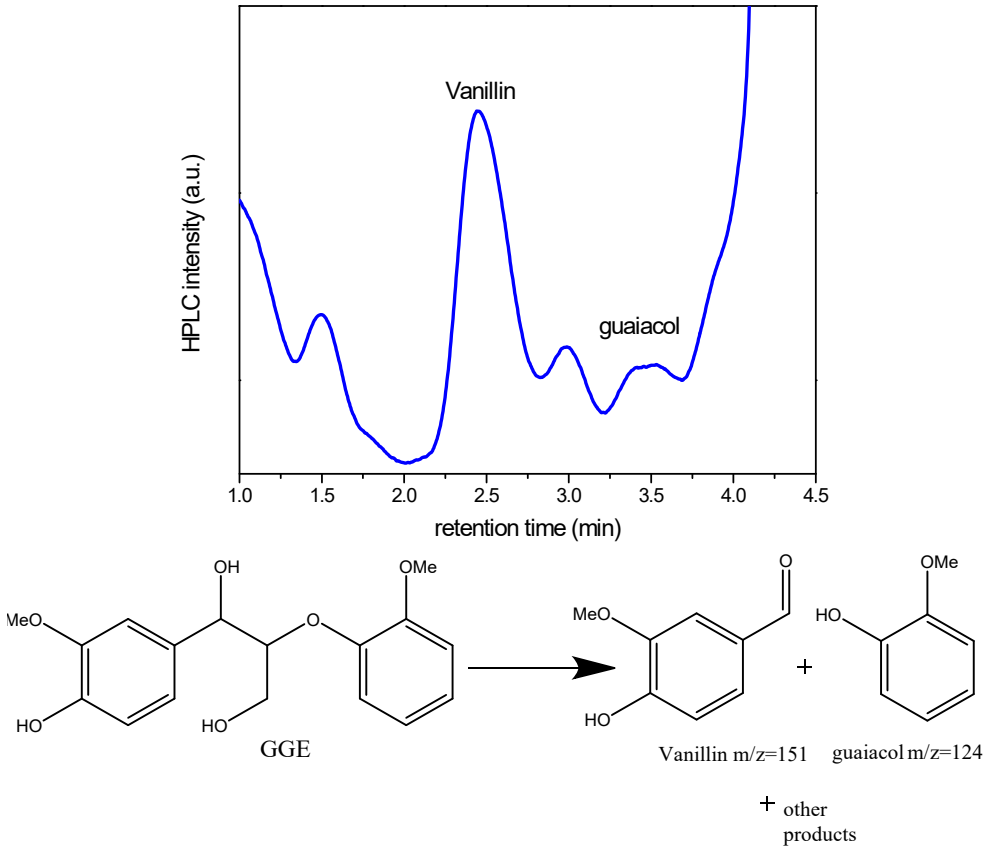

Figure S8. LC chromatogram of GGE conversion for Fe-TiO_2 NTs and estimated conversion products.

8. Repeatability, stability

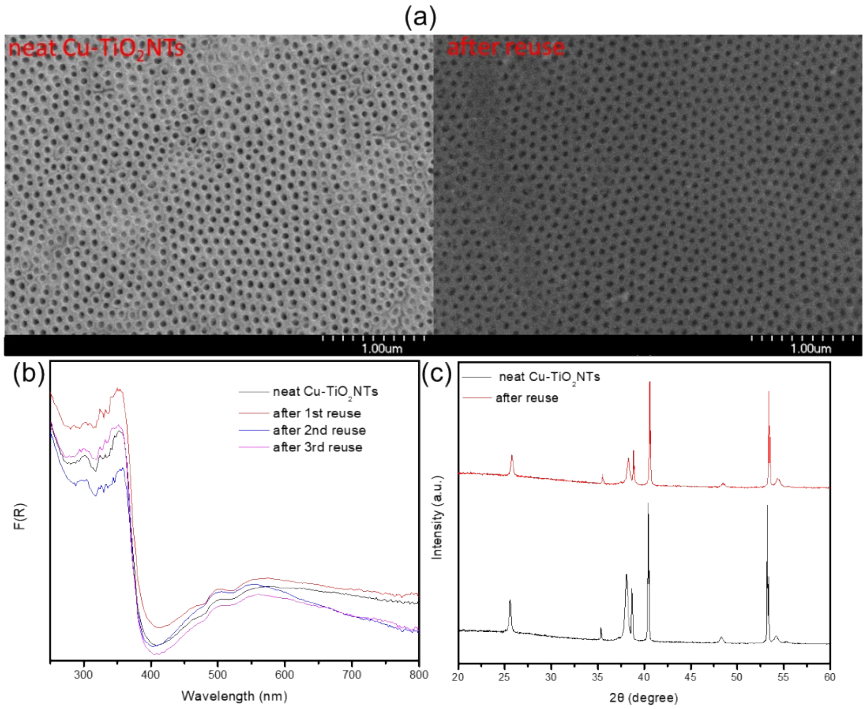

Figure S9. SEM images (a), UV-Vis spectra (b), and XRD patterns (c) of neat Cu-TiO_2 and after reuse.

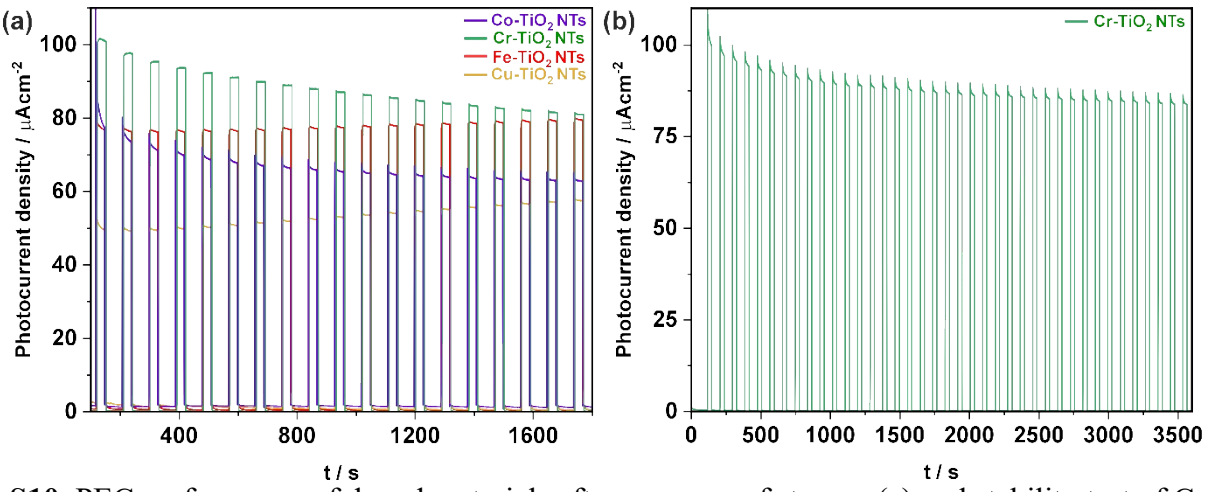

Figure S10. PEC performance of doped materials after one year of storage (a) and stability test of Cr-TiO_2 NTs material (b).

Table S2. Literature review on photocatalytic lignin decomposition - state of the art.

Photocatalyst	Lignin type	Solvent	Light	Lignin conversion %	Products	Ref
TiO_2 derived from MIL-25 Mesoporous structure regular pancake-like morphology	Sodium lignosulfonate	Aq.	300 W Xenon lamp λ=350–780 nm	2.1 mg g^{-1}_{lignin} /6h	Vanillin	1
Bi-Pt/TiO_2	Sodium lignosulfonate	Aq.	UV–Vis 125 mW/cm^2 Batch reactor	84.5/ 1.5 h 5 mg g^{-1}_{lignin} /1h	Lignin conversion Vanillin Guaiacol (22.7%/1 h), vanillic acid, 4-phenyl-1-buten-4-ol	2
Pancake-like 3D-flower morphology of BiOI-TiO_2 nanoparticles	Sodium lignosulfonate	Aq.	300 W Xenon (λ> 400 nm)	5.8 mg g^{-1}_{lignin} /6h	Vanillin	3
$Cd_xZn_{1-x}S$ Stacked layered structure	Alkali lignin	Acetonitrile+water	Simulated sunlight 300 W Xe-lamp,	89.5%/3 h 46.5 mg g^{-1}_{lignin} /7 h	Vanillin Phenol (66.2%) and acetophenone (33.5%)	4
TiO_2-NiO core-shell	Kraft lignin	Alkaline solution	UV–vis light (320–780 nm)	89.2%/ 12 h	Palmitic acid (35%), stearic acid (25%) and butanedioic acid	5

					(7%)	
TiO_2/lignin	Kraft lignin	acetonitrile	400 W Hg lamp (λmax = 365 nm)	40.28%/5 h	Aromatic aldehydes, ketones, alcohols and phenolic derivatives	6
(Fe, Cr, Co and Cu)M-doped TiO_2 NTs	Alkali lignin (Kraft)	Acetonitrile+water	UV–Vis 110 mW/cm^2	100%/12 h 9.2 μg·g_{lignin}^{-1}	Lignin conversion Vanillin concentration	This work

References

(1) J. Qiu, D. Dai, L. Zhang, M. Li, J. Xu, J. Yao, Photocatalytic conversion of sodium lignosulfonate into vanillin using mesoporous TiO_2 derived from MIL-125. Micropor. Mesopor. Mater. 319 (2021) 111043. https://doi.org/10.1016/j.micromeso.2021.111043.

(2) J. Gong, I. Alexander, F. Ramin, The promoting role of bismuth for the enhanced photocatalytic oxidation of lignin on Pt-TiO_2 under solar light illumination. Appl. Catal. B: Environ. 204 (2017) 296-303. https://doi.org/10.1016/j.apcatb.2016.11.045.

(3) J. Qiu, D. Dai, L. Zhang, Y. Zhou, L. Yang, J. Yao, Inlaying metal-organic framework derived pancake-like TiO_2 into three-dimensional BiOI for visible-light-driven generation of vanillin from sodium lignosulfonate. J. Colloid Interface Sci. 605 (2022) 648-656. https://doi.org/10.1016/j.jcis.2021.07.131.

(4) J. Xu, M. Li, J. Qiu, X.F. Zhang, J. Yao, Fine tuning of $Cd_xZn_{1-x}S$ for photo-depolymerization of alkaline lignin into vanillin. Int. J. Biol. Macromol. 185 (2021) 297-305. https://doi.org/10.1016/j.ijbiomac.2021.06.104.

(5) H. Zhao, C.F. Li, L.Y. Liu, B. Palma, Z.Y. Hu, S. Renneckar, S. Larter, Y. Li, M.G. Kibria, J. Hu, B.L. Su, np Heterojunction of TiO_2-NiO core-shell structure for efficient hydrogen generation and lignin photoreforming. J. Colloid Interface Sci. 585 (2021) 694-704. https://doi.org/10.1016/j.jcis.2020.10.049.

(6) N. Srisasiwimon, S. Chuangchote, N. Laosiripojana, T. Sagawa, TiO_2/lignin-based carbon composited photocatalysts for enhanced photocatalytic conversion of lignin to high value chemicals. ACS Sustain. Chem. Eng. 6 (2018) 13968-13976. https://doi.org/10.1021/acssuschemeng.8b02353.